



Exploring the AGN–Ram Pressure Stripping Connection in Local Clusters

Giorgia Peluso^{1,2} , Benedetta Vulcani¹ , Bianca M. Poggianti¹ , Alessia Moretti¹ , Mario Radovich¹ , Rory Smith³ , Yara L. Jaffé⁴ , Jacob Crossett⁴, Marco Gullieuszik¹ , Jacopo Fritz⁵ , and Alessandro Ignesti¹

¹INAF-Padova Astronomical Observatory, Vicolo dell'Osservatorio 5, I-35122 Padova, Italy

²Dipartimento di Fisica e Astronomia “G. Galilei”, Università di Padova, Vicolo dell'Osservatorio 3, I-35122 Padova, Italy

³Korea Astronomy and Space Science Institute (KASI), 776 Daedeokdae-ro, Yuseong-gu, Daejeon 34055, Republic of Korea

⁴Instituto de Física y Astronomía, Facultad de Ciencias, Universidad de Valparaíso, Avda. Gran Bretaña 1111, Casilla 5030, Valparaíso, Chile

⁵Instituto de Radioastronomía y Astrofísica, UNAM, Campus Morelia, A.P. 3-72, C.P. 58089, Mexico

Received 2021 October 2; revised 2021 November 3; accepted 2021 November 3; published 2022 March 9

Abstract

Ram pressure stripping (RPS) by the intracluster medium is one of the most advocated mechanisms that affect the properties of cluster galaxies. A recent study based on a small sample has found that many galaxies showing strong signatures of RPS also possess an active galactic nucleus (AGN), suggesting a possible correlation between the two phenomena. This result has not been confirmed by a subsequent study. Building upon previous findings, here we combine MUSE observations conducted within the GASP program and a general survey of the literature to robustly measure the AGN fraction in ram-pressure-stripped cluster galaxies using Baldwin–Phillips–Terlevich emission line diagrams. Considering a sample of 115 ram-pressure-stripped galaxies with stellar masses $\geq 10^9 M_{\odot}$, we find an AGN fraction of $\sim 27\%$. This fraction strongly depends on stellar mass: it raises to 51% when only ram-pressure-stripped galaxies of masses $M_{*} \geq 10^{10} M_{\odot}$ are considered. We then investigate whether the AGN incidence is in excess in ram-pressure-stripped galaxies compared to nonstripped galaxies using as a comparison a sample of noncluster galaxies observed by the MaNGA survey. Considering mass-matched samples, we find that the incidence of AGN activity is significantly higher (at a confidence level $>99.95\%$) when RPS is in the act, supporting the hypothesis of an AGN–ram pressure connection.

Unified Astronomy Thesaurus concepts: Galaxy environments (2029); Extragalactic astronomy (506); Galaxy clusters (584); Active galactic nuclei (16); Galaxy properties (615); Galaxy masses (607)

Supporting material: machine-readable tables

1. Introduction

Both theoretical and observational studies concur that there is a strong connection between the presence of an active galactic nucleus (AGN) and the host galaxy properties (see Kormendy et al. 2013, and references therein), suggesting that internal processes might regulate the AGN activity and, conversely, the AGN activity might be relevant for shaping galaxy properties. AGNs are preferentially found in more massive galaxies ($M_{*} > 10^9 M_{\odot}$; see, e.g., Kauffmann et al. 2003; Decarli et al. 2007; Juneau et al. 2011; Pimblet et al. 2013; Sabater et al. 2013; Lopes et al. 2017; Rodríguez del Pino et al. 2017; Sánchez et al. 2018) and the mass of the host galaxy is the main parameter driving the level of AGN activity (Magliocchetti et al. 2020). However, it is still debated if other factors, such as dense galaxy environment or galaxy clusters (e.g., Pimblet et al. 2013) have an impact on the presence of AGNs in galaxies.

Despite the vast literature on this topic (e.g., Kauffmann et al. 2004; Best et al. 2007; Silverman et al. 2009; von der Linden et al. 2010; Hwang et al. 2012; Martini et al. 2013; Sabater et al. 2013; Ehlert et al. 2014; Silverman & David 2015; Coldwell et al. 2017; Lopes et al. 2017; Marziani et al. 2017; Argudo-Fernández et al. 2018; Gordon et al. 2018; Koulouridis et al. 2018; Magliocchetti et al. 2018), different studies have reached quite opposite results, most likely due to the different techniques adopted to identify

AGNs, select the samples, and characterize the environment. Using a spectroscopic sample, Dressler et al. (1985) first suggested that the fraction of AGNs in clusters ($\sim 1\%$) is significantly lower than in the field ($\sim 5\%$). Similarly, Lopes et al. (2017), identifying AGNs in the Sloan Digital Sky Survey (SDSS) using optical emission lines and Baldwin–Phillips–Terlevich (BPT; Baldwin et al. 1981) diagrams, found that AGNs favor environments typical of the field, low-mass groups, or cluster outskirts. Using the same data set but a different cluster sample, von der Linden et al. (2010) showed instead that the AGN fraction does not change as a function of environment, nor of clustercentric distance (see also Miller et al. 2003). Similar conclusions were obtained by Martini et al. (2007), Lehmer et al. (2007), Sivakoff et al. (2008), and Arnold et al. (2009), exploiting X-ray data. Yet, the radio AGN fraction seems to be much higher in clusters than in the field (Best et al. 2007; Sabater et al. 2013).

Considering local density as a proxy for environment, Kauffmann et al. (2004) found that AGN host galaxies with strong [O III] emission are twice as frequent in low-density regions than in high-density regions (see also Miller et al. 2003; Montero-Dorta et al. 2009). In contrast, Amiri et al. (2019) did not find any effect of the galaxy density on nuclear activity. Sabater et al. (2013) found that (at fixed mass) the prevalence of optical AGNs is a factor of 2–3 lower in the densest environments (see also Man et al. 2019), but increases by a factor of ~ 2 in the presence of strong one-on-one interactions. Gilmour et al. (2007) showed that X-ray-selected AGNs lie predominantly in moderate dense regions.

The expected connection between AGN incidence and properties with the environment has roots in the fact that the



Original content from this work may be used under the terms of the [Creative Commons Attribution 4.0 licence](https://creativecommons.org/licenses/by/4.0/). Any further distribution of this work must maintain attribution to the author(s) and the title of the work, journal citation and DOI.

characteristics of AGNs are strongly linked to the conditions of the available gas, which in turn can be affected by the galaxy environment. So any environmentally specific physical mechanism that has the potential to affect the galaxy gas can impact the AGN activity. For example, mergers—which most frequently happen in the field—have frequently been cited as a method to fuel AGNs (e.g., Sanders et al. 1988) and a number of morphological studies claim an excess of post-merger systems in their AGN samples (Bahcall et al. 1997; Canalizo & Stockton 2001; Urrutia et al. 2008; Letawe et al. 2010; Smirnova et al. 2010).

Another process able to affect the gas supply in galaxies is ram pressure stripping (RPS; Gunn et al. 1972). This mechanism happens most efficiently in clusters and massive groups (Hester 2006) and it is due to the pressure exerted by the intracluster medium (ICM) on the galaxy interstellar medium (ISM). This interaction can produce many visible effects on the galaxy, such as altering its less-bound gas, giving rise to wakes of stripped material departing from the main galaxy body (Kenney et al. 2004; van Gorkom 2004; Fumagalli et al. 2014; Poggianti et al. 2017a) and inducing a quenching of star formation (Vollmer et al. 2001; Tonnesen et al. 2007; Vulcani et al. 2020). Prior to complete gas removal, it has been observed that ram pressure can also increase the star formation rate in galaxies (Crowl & Kenney 2006; Merluzzi et al. 2013; Vulcani et al. 2018) and simulations support this finding (Kronberger et al. 2008; Kapferer et al. 2009; Tonnesen et al. 2009; Bekki 2014), suggesting that the increased pressure initially helps compress the gas and triggers increased star formation. The same mechanism that initially promotes star formation can also fuel the AGN during the RPS process: gas can be funneled toward the galaxy centers due to gravitational instabilities and the spiraling toward the center of clumps that lose angular momentum (Schulz & Struck 2001; Tonnesen et al. 2009; Ramos-Martínez et al. 2018). The funneling of gas toward the galaxy center can also ignite the central supermassive black hole. Theoretical models (Tonnesen et al. 2009) have indeed demonstrated that gas inflows can fuel the central AGN in ram-pressure-stripped galaxies, possibly due to the presence of magnetic fields (Ramos-Martínez et al. 2018). The enhanced accretion onto the black hole can then produce heating and outflows due to AGN feedback (Ricarte et al. 2020).

Therefore RPS might be simultaneously responsible for an enhanced AGN activity and the appearance of tails of stripped material. This scenario has been first proposed by Poggianti et al. (2017b, hereafter P17b) to explain the very high incidence (6/7) of AGN detected in a sample of galaxies strongly affected by RPS, also called jellyfish galaxies (see also Maier et al. 2022). That analysis is based on integral-field spectroscopic data coming from the Gas Stripping Phenomena (GASP) in galaxies (Poggianti et al. 2017a). Subsequent GASP studies have led to the identification of AGN-driven outflows (Radovich et al. 2019) and a compelling case for AGN feedback in action (George et al. 2019).

The P17b analysis is based on a small sample and importantly is only composed of jellyfish galaxies with very striking tails and all massive galaxies. Thus, it leaves open the possibility that the AGN activity could be only related to the (rather short) peak phase of stripping and/or only to the galaxy mass regardless of RPS.

A subsequent study that did not find a high incidence of AGNs (Roman-Oliveira et al. 2018)⁶ analyzed a sample of ram-pressure-stripped galaxies in a supercluster at $z \sim 0.2$ and found only 5/70 AGN, according to optical line diagnostics. Their sample spans a wide galaxy stellar mass range (from 10^9 to $10^{11.5} M_{\odot}$) and is based on visual identification of the candidates. At odds with GASP, none of these candidates have IFS data to confirm they are indeed affected by RPS. It also includes RPS candidates with different degrees of stripping, while as said above the P17b study includes only very dramatic cases.

In this paper, we build on previous results and aim at estimating the incidence of AGN on the largest possible sample of ram-pressure-stripped galaxies to date.

Throughout the paper, we adopt a Chabrier (2003) initial mass function (IMF) in the mass range $0.1\text{--}100 M_{\odot}$. The cosmological constants assumed are $\Omega_m = 0.3$, $\Omega_{\Lambda} = 0.7$, and $H_0 = 70 \text{ km s}^{-1} \text{ Mpc}^{-1}$.

2. Data sets and Galaxy Samples

In this paper we aim at characterizing the incidence of AGN activity among ram-pressure-stripped cluster galaxies. We start our analysis by considering a sample of galaxies drawn from the GASP (Poggianti et al. 2017a) survey, then, to increase the statistics and more robustly support the results, we also gather a literature sample of all ram-pressure-stripped galaxies identified by different authors in the last four decades. Finally, we exploit the fifteenth data release of the MaNGA survey (DR15; Aguado et al. 2019) to build a control sample of galaxies with characteristics similar to the ram-pressure-stripped galaxies, but considering only those *not* in clusters and therefore presumably not affected by strong RPS.

2.1. The GASP Sample and Data

GASP is a project aimed at studying gas removal processes, mainly due to ICM–ISM interaction, using a sample of 114 galaxies. More specifically, it comprises both RPS candidates and undisturbed galaxies located in clusters, groups, and field, spanning a range in stellar masses from 10^9 to $3.2 \times 10^{11} M_{\odot}$ and a redshift range of $0.04 < z < 0.07$. All galaxies were selected on the basis of *B*-band imaging coming from three different surveys: WINGS (Fasano et al. 2006), OMEGAWINGS (Gullieuszik et al. 2015), and PM2GC (Calvi et al. 2011).

GASP is based on an ESO Large Program carried out with the integral-field spectrograph MUSE, mounted at the VLT, whose large field of view ($1' \times 1'$) and high, but seeing-limited, spatial resolution ($0''.2 \text{ pixel}^{-1}$, seeing of $1''$), allow us to cover the galaxy outskirts and possible tails of gas departing from the main body of the galaxies up to ten times the galaxy effective radius (i.e., $\sim 10 R_e$) with a resolution of $\sim 1 \text{ kpc}$ at the galaxy redshifts.

For our analysis, we select only cluster members that have been confirmed to be ram pressure stripped based on the MUSE data; in fact, they all have extraplanar $H\alpha$ emission in various stages of stripping (B. Poggianti et al. 2021, in preparation), from weak/initial stripping (JStage = 0.5) to significant tails (JStage = 1) to extreme tails longer than the stellar disk diameter (JStage = 2, so-called jellyfish galaxies) to truncated disks corresponding to a late stage of RPS (Jstage = 3), for a

⁶ See also Boselli et al. (2021) which appeared unrefereed on astro-ph on September 28 2021.

total of 51 galaxies. From now on we will call this sample GASP-RPS. All of these are morphologically late-type and star-forming galaxies.

We make use of the fluxes of the emission-only component of the lines $H\alpha$, $H\beta$, $[O\text{ III}]\lambda\ 5007\text{ \AA}$ and $[N\text{ II}]\lambda\ 6583\text{ \AA}$ measured with the KUBEVIZ code (Fossati et al. 2016) from the continuum-subtracted MUSE cubes corrected for both Galactic and intrinsic extinction, as described in detail in Poggianti et al. (2017a). Stellar masses are taken from Vulcani et al. (2018) and are computed using the SINOPSIS spectrophotometric code (Fritz et al. 2017) by summing up the masses of all the spaxels within the galaxy disk (Gullieuszik et al. 2020).

To characterize the ionization mechanism acting on the gas and therefore identify galaxies with AGNs, we inspect the BPT diagnostic diagram $[N\text{ II}]/H\alpha$ versus $[O\text{ III}]/H\beta$ ratios (BPT-N II; Baldwin et al. 1981). We consider only spaxels with a signal-to-noise (S/N) ratio greater than 3 for all the lines used. We use the relation from Kauffmann et al. (2003) (K03) to separate star-forming from composite regions, the Kewley et al. (2001) (K01) line to identify AGNs,⁷ and the Sharp et al. (2010) (SB10) relation to discriminate between Seyferts and LINERs. We classify a galaxy as an AGN host if in its central ($3''$) region there are at least 20 spaxels⁸ that have a Seyfert or LINER classification, otherwise we flag it as star-forming. In the galaxies with high values of extinction (A_V , as measured by the Balmer decrement) in the central cores, that might prevent us from identifying an AGN, we further inspect the LINER classified spaxels: a biconical shape of their distribution suggests extended ionized regions and therefore indicates the presence of the AGN.

For those galaxies with a central LINER/AGN classification, we have carefully checked the emission line fits, in particular the $H\beta$ line given that an underestimate of $H\beta$ flux would lead to an overestimate of the $[O\text{ III}]/H\beta$ ratio, mimicking line ratios typical of AGNs.

2.2. Ram Pressure Stripping Candidates from the Literature

We have performed a systematic literature search of all the ram-pressure-stripped galaxies identified by 2020 December. These galaxies were studied exploiting a wide variety of observational techniques, including radio (e.g., Gavazzi et al. 1995), submillimeter (e.g., Scott et al. 2013; Jáchym et al. 2014, 2019), infrared (e.g., Sivanandam et al. 2010, 2014), optical (e.g., Gavazzi et al. 1995, 2001; Sun et al. 2007; Sivanandam et al. 2010; Sun et al. 2010; Yagi et al. 2010; Fumagalli et al. 2014; Fossati et al. 2016; Gavazzi et al. 2017; Roberts et al. 2020), UV (e.g., Smith et al. 2010), and X-ray (e.g., Sun et al. 2006, 2010). The assembled sample is therefore greatly heterogeneous and while for some galaxies it has been confirmed that RPS is the only acting mechanism, in some other cases galaxies are most likely undergoing both RPS and tidal interactions. As our aim is to include all ram-pressure-stripped galaxies and collect a sample as large as possible, we

⁷ The choice of the K01 demarcation line to identify AGNs is a conservative choice that minimizes the AGN spaxels. Note that recent works (see Law et al. 2021 and references therein) find a demarcation line in the N II-BPT diagram closer to the K03 separation, but we choose the most conservative one to minimize the contamination from star-forming regions.

⁸ We adopted this number upon visual inspection of the maps. This choice allows us to have enough spaxels to identify possible AGNs with high confidence, still focusing on the central part of the galaxy.

consider also the latter cases. However, we remove cases where a merger or tidal interaction is the main cause of the galaxy transformation.⁹

We narrow down our search to galaxies for which we retrieve information at any wavelength on the ionization mechanism of the central emission,¹⁰ obtaining a total sample of 80 galaxies (from now on LIT-RPS sample). All these turn out to have some active star formation (in addition to the eventual AGN activity) in the available literature.

The LIT-RPS sample is located in the redshift range $0.001 \leq z \leq 0.34$, plus a galaxy at $z = 0.73$, and covers a stellar mass range of $1.3 \times 10^8 < M_*/M_\odot < 2.0 \times 10^{11}$. Stellar masses have been collected from the literature and homogenized to the same Chabrier (2003) IMF (as in GASP). When a stellar mass estimate was not available (4/80), we computed it using the available photometric data following the Bell et al. (2001) approach, as described in the Appendix.

To assess the strength of RPS signatures and compare them with the GASP JStage classification, four of us (GP, BMP, BV, AM) visually inspected the available images in the literature for all the galaxies. Following the scheme described in Section 2.1, we assign a flag indicating the extent of the tail (JStage) based on the $H\alpha$ emission (if available) and also a general JStage based on any wavelength observed ($JStage_{gen}$). In the case of multiple images with different resolutions or at different wavelengths showing a different extent of the tail, we always consider the wavelength with the longest visible tail to assign the $JStage_{gen}$. The classifiers agreed in most of the cases. In the discrepant cases, each galaxy was inspected together by the classifiers to ensure homogeneity and to find a consensus. This visual inspection also confirmed that the LIT-RPS sample is composed of morphologically late-type galaxies (spirals or irregulars).

2.3. The MaNGA Sample

Mapping Nearby Galaxies at Apache Point Observatory (MaNGA; Bundy 2015) is an integral-field spectroscopic survey observing galaxies at $0.01 \leq z \leq 0.15$ using the BOSS Spectrograph (Smee et al. 2013) mounted at the 2.5 m SDSS telescope (Gunn et al. 2006), which covers a spectral range from 3600 to 10300 Å, with a resolution of $R \sim 1400$ at 4000 Å and $R \sim 2600$ at 9000 Å.

We exploit the MaNGA DR15 release and use the outputs of the Pipe3D pipeline (Sánchez et al. 2016a, 2016b, 2018). More specifically, we use the Pipe3D-v2_4_3¹¹ catalog, which contains integrated properties, characteristics, and gradients of different quantities for 4656 galaxies. Of interest for our work are integrated stellar masses and star formation rates obtained from the $H\alpha$ emission line that we convert to our adopted Chabrier (2003) IMF.

We first exclude from the sample 75 duplicate galaxies and then select only galaxies with a specific star formation rate ($sSFR$) $> 10^{-11} \text{ yr}^{-1}$, for a total of 2509 galaxies. The latter

⁹ The candidate merging systems removed from the sample are F0237 (Owers et al. 2012), NGC 4294, NGC 4299, and NGC 4302 (Pappalardo et al. 2012; Vollmer et al. 2013).

¹⁰ A list of all ram-pressure-stripped galaxies known in the literature, regardless of AGN information, will be published in J. Crossett et al. 2021, in preparation.

¹¹ https://www.sdss.org/dr16/data_access/value-added-catalogs/?vac_id=manga-pipe3d-value-added-catalog:-spatially-resolved-and-integrated-properties-of-galaxies-for-dr15

selection allows us to consider only star-forming galaxies, as are galaxies in both the GASP-RPS and LIT-RPS samples.

As we aim at assembling a sample not affected by RPS, we crossmatch our sample with the environmental catalog by Tempel et al. (2014), who provide halo mass estimates based on Navarro et al. (1997) profiles. Using a searching radius of $5''$, we obtain a match for 2061 galaxies, 861 of which are located in structures with halo masses $\log(M_h/M_\odot) < 13.0$,¹² therefore are most likely isolated (Yang et al. 2007).

Finally, to reduce the effect of a different morphological mix among the different samples, we use the visual morphological classification from the MaNGA Value Added Catalogs¹³ that is based on inspection of image mosaics using a new reprocessing of SDSS and Dark Energy Legacy Survey (DESI) images, following the methods from Hernández-Toledo et al. (2010) and exclude 70 early-type (Ellipticals, S0s, and S0as) and two unclassified galaxies.¹⁴

To assemble the final MaNGA sample, we consider only galaxies that in a circular aperture of $3''$ diameter (i.e., the SDSS fiber size) centered on the galaxy have at least 20 spaxels with $S/N > 3$ for all lines that will be used to detect the presence of an AGN. 782 galaxies pass this selection and constitute our reference sample, called MaNGA-Ref. This sample covers a redshift range $0.0024 < z < 0.1439$. We note that the MaNGA fiber core diameter ($2''$) is similar to the typical seeing value ($2''.5$). At the median redshift of our MaNGA-Ref sample ($z = 0.0317$), the MaNGA spatial resolution of $2''$ corresponds to 1.27 kpc and at the 75% redshift percentile ($z = 0.043$) to 1.7 kpc. This is only slightly worse than the GASP spatial resolution of ~ 1 kpc (median $z = 0.05$), which is dominated by the seeing ($\sim 1''$).¹⁵

To identify AGN, we inspect the BPT-N II maps provided by the online tool MARVIN¹⁶ and use the same classification criteria as for the RPS samples. We count the number of spaxels classified as AGN (i.e., Seyfert + LINER), star-forming (SF), or composite. If the number of spaxels classified as Seyfert or LINER is larger than 20 in a circular aperture of $3''$ diameter, we classify the galaxy as AGN, otherwise as SF.

3. Results I: The Incidence of AGN among Ram-pressure-stripped Galaxies

In this section we present the sample of AGN hosts in the GASP-RPS and in the LIT-RPS samples separately and quantify the incidence of AGNs among ram-pressure-stripped galaxies. We also investigate if these fractions depend on the properties of the ram-pressure-stripped galaxies, such as stellar mass and Jstage. In the following section we will quantitatively compare these fractions controlling for the different mass distribution to those of the MaNGA-Ref sample.

¹² We verified that results are insensitive to the exact choice of this threshold, exploring log halo masses up to 13.6. We decided to use a conservative cut (13.0) to avoid the possibility that ram-pressure-stripped galaxies in groups contaminate the sample.

¹³ https://www.sdss.org/dr16/data_access/value-added-catalogs/?vac_id=manga-visual-morphologies-from-sdss-and-desi-images

¹⁴ For consistency with the other samples, we have applied the morphological cut, but all the results remain unchanged if no morphological criterion is applied.

¹⁵ This is why in GASP the data cubes have been filtered with a 5×5 kernel (Poggianti et al. 2017a).

¹⁶ <https://www.sdss.org/dr15/manga/marvin/>

3.1. GASP-RPS

In the GASP-RPS sample, seven galaxies are already known to host an AGN; six of them were presented in P17b and one (JO36), in Fritz et al. (2017). The latter is an edge-on disk hosting an obscured AGN which is not directly identified using BPT diagrams due to strong dust absorption. However, evidence for the AGN presence comes from extra-nuclear LINER-like emission with a cone morphology and the AGN is detected by Chandra as a point-like X-ray source (Fritz et al. 2017).

Among the P17b candidates, JO194 was classified as a LINER and its combined line ratios are better reproduced by an AGN model (Radovich et al. 2019), while JO201, JO206, JO204, JW100, and JO135 are classified as Seyfert galaxies according to BPT diagrams and are all Seyfert 2. JO204 and JO135 also have extended emission line regions ionized by the AGN. Four of these galaxies display AGN outflows (Radovich et al. 2019).

Having inspected all other GASP cluster member ram-pressure-stripped galaxies, we find other five AGN candidates that are presented in Figure 1. The stripping characteristics of these galaxies were discussed in previous works and only summarized here, but the analysis of their central ionization mechanism is shown here for the first time. JO49 has unwinding tails due to RPS (Bellhouse et al. 2021). It presents a central LINER-like region surrounded by a thin composite-like ring, which in the BPT diagram corresponds to a long finger of points encompassing the composite region extending well beyond the K01 line. We note that JO49 hosts also an X-ray source of luminosity $1.2 \times 10^{41} \text{ erg s}^{-1}$, detected by XMM-Newton (Webb et al. 2020)¹⁷.

JO85, another unwinding ram-pressure-stripped galaxy (Bellhouse et al. 2021), has fewer LINER-like points than JO49 embedded in a Composite-like region, but it is highly obscured by dust ($A_V \sim 2.7$ in the central region as measured by the Balmer decrement) and has a central Chandra point source with a luminosity of $5.0 \times 10^{40} \text{ erg s}^{-1}$ (Evans et al. 2020).

JO147 (first described by Merluzzi et al. 2013; see also Poggianti et al. 2019) is an inclined, highly extinguished disk and is stripped in the northwest direction. We find that it has LINER-like opposite cones embedded in wider composite cones. Its luminosity in the X-ray band observed by XMM-Newton is $2.4 \times 10^{41} \text{ erg s}^{-1}$ (Webb et al. 2020).

JO171 is a Hoag-like ring galaxy with long tails stripped in the north direction (Moretti et al. 2018). It has central AGN-powered spaxels (Seyfert 2) in the inner kpc.

Finally, JW39 has long tails originating from unwinding spiral arms (Bellhouse et al. 2021). It has a LINER-like circular central region surrounded by a larger circular area with composite emission.

The latter two galaxies have no available central X-ray counterparts, from neither XMM-Newton nor Chandra.

To summarize, with respect to the sample of AGNs described in P17b and Radovich et al. (2019), we find an additional Seyfert 2 and four LINER-like galaxies, yielding a total sample of 12 AGN hosts in the GASP-RPS sample. Their main properties are summarized in Table 1.

¹⁷ The 4XMM-DR10 catalog contains source detections covering an energy interval from 0.2 keV to 12 keV. On the other hand, the Chandra energy range goes from 0.5 to 7 keV.

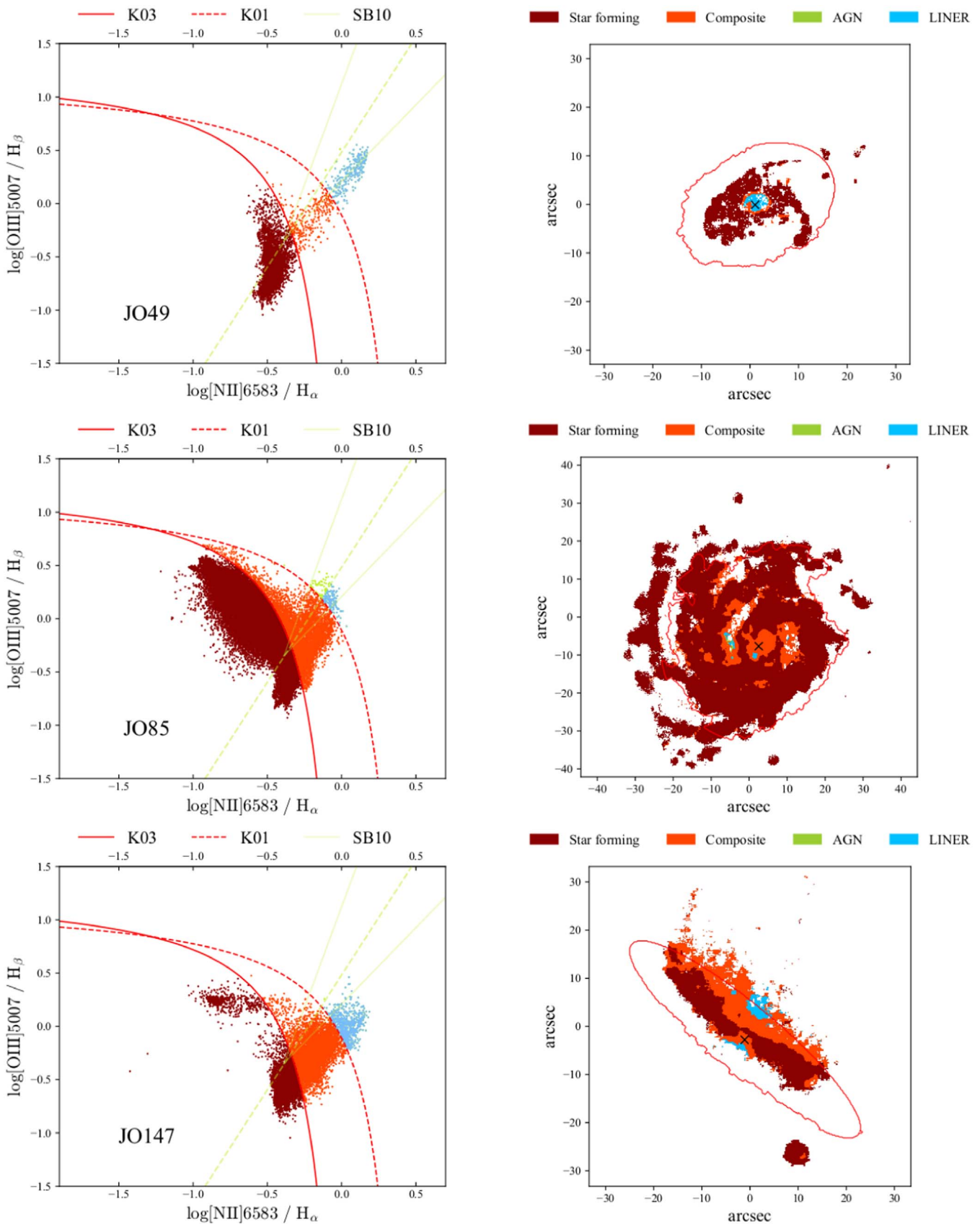


Figure 1. Left: BPT-NII diagnostic diagram for all spaxels with $S/N > 3$. The red dotted and continuous lines are defined as in Kewley et al. (2001) and Kauffmann et al. (2003), respectively. The green lines are taken from Sharp et al. (2010). Right: galaxy map color-coded according to the BPT-NII classification; red lines are the stellar emission isocontours corresponding to the galactic disk edges.

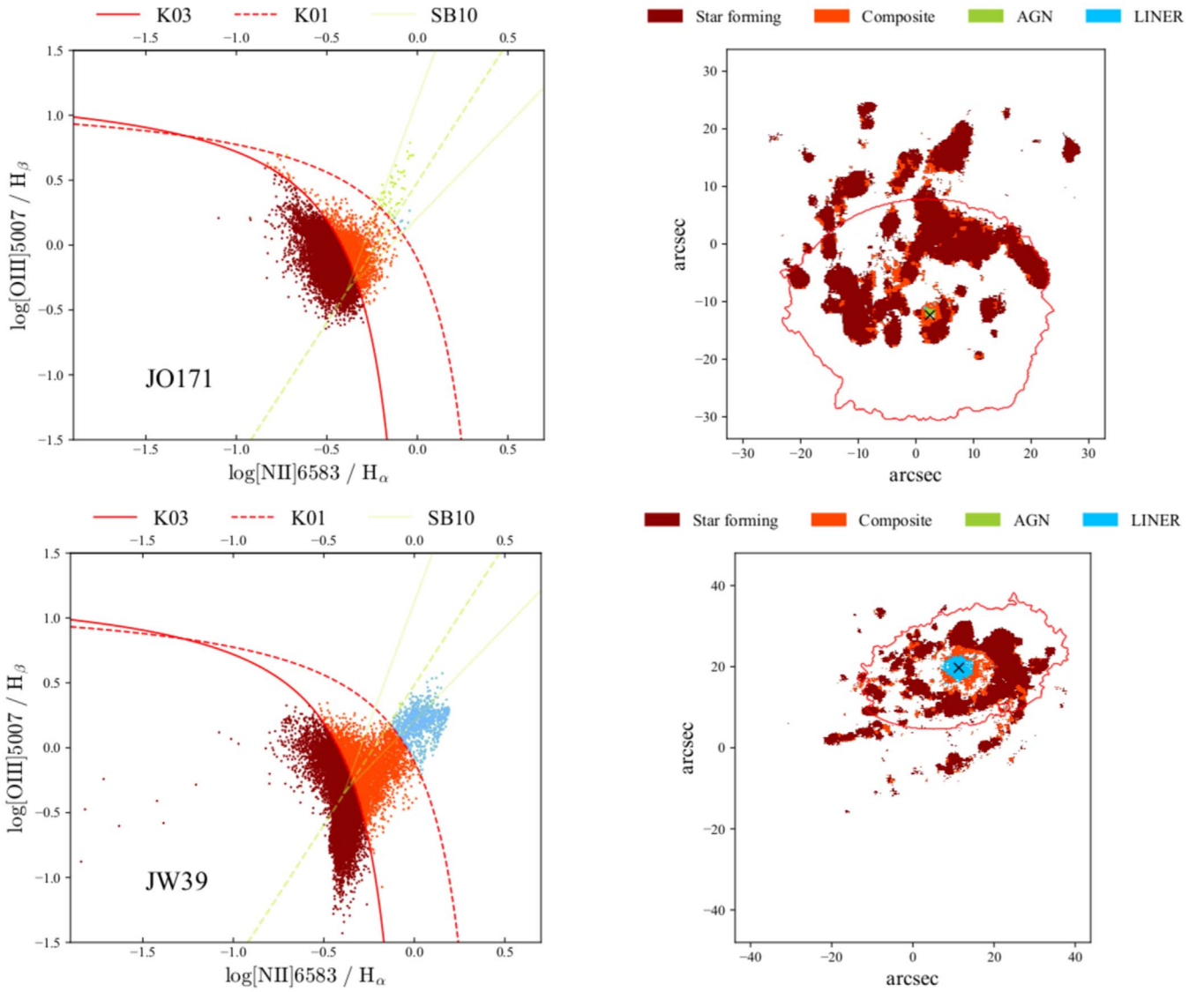


Figure 1. (Continued.)

Table 1
AGN Candidates in the GASP Sample

ID	R.A.	Decl.	z	Cluster	$\log M_*/M_\odot$	Jstage	AGN Flag	References
JO85	351.13068	16.86815	0.0355	A2589	10.7	1	3	This paper
JO36	18.247583	15.591488	0.0407	A160	10.8	3	4	Fritz et al. (2017)
JO194	359.25284	-34.680588	0.042	A4059	11.2	2	3	P17b
JO204	153.44513	-0.914182	0.0424	A957	10.6	2	2	P17b
JO201	10.376208	-9.26275	0.0446	A85	10.8	2	2	P17b
JO49	18.682709	0.286136	0.0451	A168	10.7	2	3	This paper
JO147	201.70721	-31.395975	0.0506	A3558	11.0	2	3	This paper
JO206	318.44754	2.476218	0.0511	IIZW108	11.0	2	2	P17b
JO171	302.56125	-56.641823	0.0521	A3667	10.6	2	2	This paper
JO135	194.26791	-30.375088	0.0544	A3532	11.0	2	2	P17b
JW100	354.10443	21.150702	0.0619	A2626	11.4	2	2	P17b
JW39	196.03212	19.210691	0.0663	A1668	11.2	2	3	This paper

Note. Columns: (1) GASP ID; (2–3) coordinates of the optical center; (4) galaxy redshift; (5) host cluster; (6) galaxy stellar masses (Vulcani et al. 2018); (7) Jstage (B. Poggianti et al. 2021, in preparation); (8) AGN classification; (9) works in which the source is presented. The adopted AGN flag for both GASP-RPS and LIT-RPS galaxies ranges from 0 to 6: 0 means that star formation is the dominant ionization process at the galaxy center according to BPT-N II classification; 1, 2, 3 if the galaxy hosts a Seyfert 1, Seyfert 2 or LINER-like nucleus, respectively, again according to the BPT diagram; 4 if the AGN has been detected through the X-ray signal, but not in the optical; 5 when the galaxy is classified as a radio galaxy; 6 when the source is classified as an AGN, without any specification on the type.

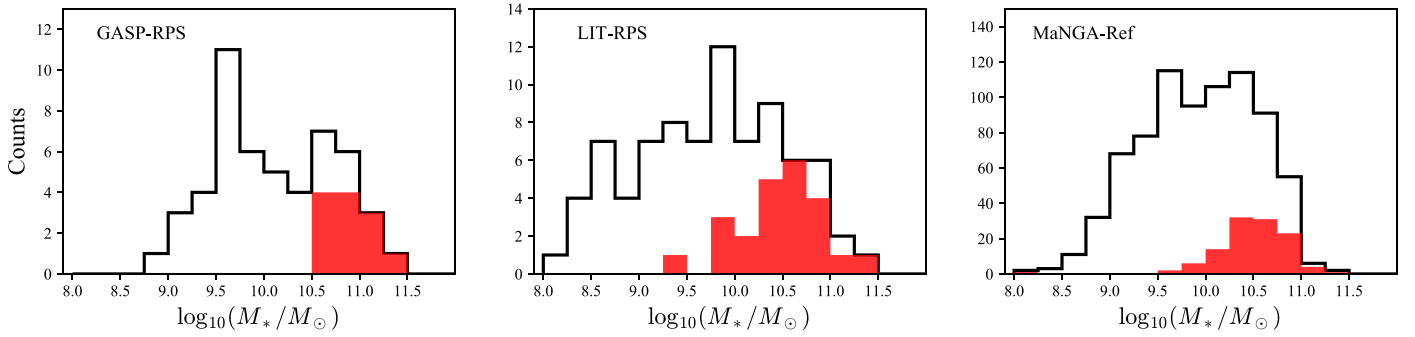


Figure 2. Stellar mass distributions for all galaxies (black histogram) and for galaxies hosting an AGN (red histogram). From left to right: the GASP-RPS, LIT-RPS, and MaNGA-Ref samples.

The left panel of Figure 2 shows the mass distribution of galaxies hosting an AGN compared to the entire GASP-RPS sample. While RPS galaxies cover a mass range of $8.7 \leq \log(M_*/M_\odot) \leq 11.5$, AGN hosts are among the most massive galaxies in the sample, having all $\log(M_*/M_\odot) \geq 10.5$.

We are now in the position of computing the fraction of AGNs (f_{AGN}) over the total (AGN+SF) number of galaxies, considering different subsamples, as summarized in Table 2. The AGN fraction in the total GASP-RPS sample is $0.24^{+0.06}_{-0.05}$, with uncertainties computed as binomial errors. Restricting the sample to $\log(M_*/M_\odot) \geq 10.5$, this fraction becomes $0.71^{+0.10}_{-0.12}$.

Considering the various stages of stripping (Figure 3), the frequency of AGNs increases with the strength of RPS signatures; no galaxies with AGN activity have $J_{\text{stage}} = 0.5$, while the AGN incidence increases among moderate stripping galaxies ($J_{\text{stage}} = 1, 8\%$) and is particularly high among $J_{\text{stage}} = 2$ galaxies, where it reaches 56%. Still one out of four galaxies in a late stage of RPS (truncated disks, $J_{\text{stage}} = 3$) has an AGN. Interestingly, using the same methods of the current analysis, only two AGNs are found in the GASP non-RPS sample of star-forming galaxies, which consists of 49 galaxies (Vulcani et al. 2021; B. Poggianti et al. 2021, in preparation).

In the GASP-RPS sample, out of the 17 galaxies more massive than $\log(M_*/M_\odot) \geq 10.5$, 10 ($\sim 58\%$) have $J_{\text{stage}} = 2$ and, vice-versa, $\sim 55\%$ (10/18) of the $J_{\text{stage}} = 2$ galaxies are more massive than $\log(M_*/M_\odot) \geq 10.5$. All of them host an AGN. It is significant that none of the massive galaxies have a $J_{\text{stage}} = 0.5$. This result suggests a tight correlation between stellar mass and J_{stage} . The correlation is probably linked with the higher capability of massive galaxies to retain gas. While low-mass galaxies are already completely stripped when they approach the densest regions in clusters, high-mass galaxies more easily hold onto their gas (Jaffé et al. 2018; Luber et al., submitted to ApJ) and experience RPS in these dense regions, where the gas removal is the most intense. Since AGNs are preferentially located in the most stripped and massive galaxies, we cannot state which of these two parameters is more connected to the presence of an AGN.

3.2. LIT-RPS

The catalog of the 82 literature ram-pressure-stripped galaxies with SF/AGN information is presented in Table 3. Stellar masses and AGN classification, along with the source for those values are given in Table 4.

One of these galaxies has broad optical lines typical of Seyfert 1. For all the other galaxies the AGN classification is based on the BPT-N II diagnostic. For $\sim 68\%$ (55/81) of them

Table 2
AGN Fractions in the GASP-RPS Sample

$N_{\text{AGN}}/N_{\text{TOT}}$	f_{AGN}	J_{stage}	$\log(M_*/M_\odot)$
12/51	$0.24^{+0.06}_{-0.05}$	≥ 0.5	All
12/17	$0.71^{+0.10}_{-0.12}$	≥ 0.5	≥ 10.5
0/16	$0.0^{+0.06}_{-0.0}$	$= 0.5$	All
1/13	$0.08^{+0.11}_{-0.05}$	$= 1$	All
10/18	$0.56^{+0.11}_{-0.12}$	$= 2$	All
1/4	$0.25^{+0.25}_{-0.15}$	$= 3$	All

Note. Considering galaxies of different mass, and characterized by different J_{stage} s. Errors are binomial.

the classification in published results is based on spectroscopic observations published in dedicated papers, either from the integral-field unit (Merluzzi et al. 2013; Fossati et al. 2016; Merluzzi et al. 2016; Consolandi et al. 2017; Boselli et al. 2019; Stroe et al. 2020), long-slit or fiber spectra (Véron-Cetty & Véron 2003; Owen et al. 2006; Cortese et al. 2007; Mahajan et al. 2010¹⁸; Owers et al. 2012; Ebeling et al. 2019). For the other 32% (26/81) of the galaxies, we instead use the online AGN classification based on the analysis of emission line ratios extracted from integrated spectra of the central circular aperture ($r \sim 3''$) observed with the SDSS fiber (Data Release 8, from now on DR8; Aihara et al. 2011) as analyzed by Brinchmann et al. (2004), Kauffmann et al. 2003, and Tremonti et al. (2004) in the Value Added Catalog MPA/JHU. For 24 galaxies, we had both the DR8 automatic classification and information about the central source from individual publications in the literature. In these cases we favored the latter.

We note that four of the 81 galaxies also have information coming from either X-ray or radio data (Winkler & Winkler 1992; Best et al. 2012; Owers et al. 2012; Ebeling et al. 2019; Kalita et al. 2019; Caglar et al. 2020). While their position on a BPT-N II diagram suggests they are star-forming, the additional data instead classify them as AGNs. In what follows we will therefore discuss how results change if we include or exclude these four objects.

Overall, 24/82 galaxies host an AGN ($\sim 30\%$). If we disregard the AGN classification based on X-ray or radio data and consistently consider only the BPT-N II classification, the fraction above becomes 20/82 ($\sim 24\%$).

¹⁸ We note that for two galaxies, GMP3618 and D100, Mahajan et al. (2010) give different results with respect to the classification reported in the DR7 (Abazajian et al. 2009) and DR8 (Aihara et al. 2011) analysis even though they used DR7 data to build up BPT-N II.

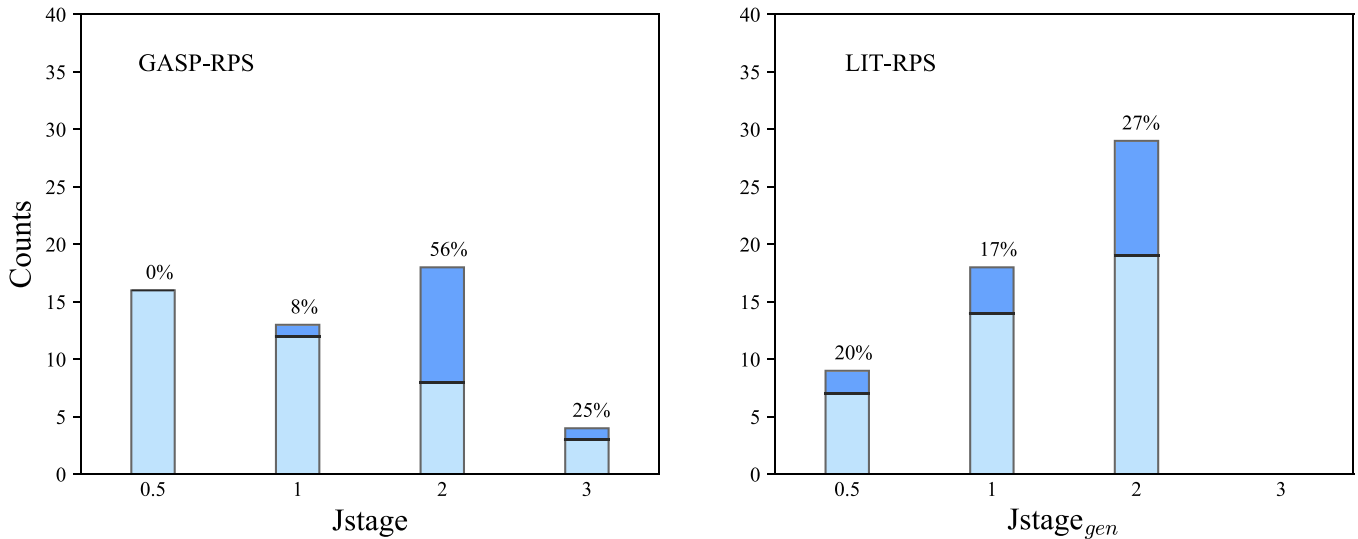


Figure 3. Stacked histograms for galaxies of different Jstages and divided among centrally star-forming galaxies (light blue histogram) and AGNs (dark blue histogram) according to the BPT-N II classification for GASP-RPS (left) and LIT-RPS (right). Percentages are AGN fractions in the corresponding bin of Jstage and Jstage_{gen}.

Table 3
Portion of the Catalog of Ram-pressure-stripped Galaxies

Name	R.A.	Decl.	z	Cluster	Jstage	Jstage _{gen}	Alternative Names
MIP001417–302303	3.5693	−30.3843	0.2955	A2744	...	2.0	F1228
HLS001427–302344	3.61065	−30.39581	0.3033	A2744	...	2.0	F0083
NGC 1566	65.00175	−54.93781	0.005	Dorado	0.0	0.0	...
ID345	149.9191	2.5281	0.727	CGr32	2.0	2.0	...
LEDA36382	175.73523	19.96621	0.02427	A1367	2.0	2.0	CGCG97073

Note. Columns: (1) galaxy name; (2) and (3) equatorial coordinates of the galaxy center from SIMBAD; (4) galaxy redshift; (5) host cluster; (6) and (7) Jstage and general Jstage, defined in Section 3.2; (8) alternative names. Stellar masses flagged with the asterisk (*) are computed by means of photometric data as described in the Appendix. This table is published in its entirety in a machine-readable format. A portion is shown here for guidance regarding its form and content.

(This table is available in its entirety in machine-readable form.)

The central panel in Figure 2 shows the mass distribution of the galaxies with and without an AGN. The entire sample spans a mass range $8.1 < \log(M_*/M_\odot) < 11.4$. Similar to what was found for GASP, most of the AGNs are massive galaxies, even though in this sample there are also a few less massive AGN hosts. Above the GASP AGN mass limit ($\log(M_*/M_\odot) > 10.5$) the AGN fraction becomes $0.80^{+0.08}_{-0.12}$.

Table 5 reports the AGN fraction for the different subsamples considered, including that for galaxies of different Jstage_{gen}. The trend of the AGN fraction with Jstage_{gen} is weaker than in GASP-RPS (see also Figure 3), with the percentages ranging between 17% and 27% but being consistent within the large errors in all Jstages_{gen}.¹⁹

We remind the reader that while the AGN classification and mass estimates among GASP galaxies are homogeneous, for the LIT-RPS sample we based the former on a number of different data and indicators. In addition, stellar masses have been computed following many different approaches and so, even though homogenized to the same IMF, there could be some systematics among the different galaxies. Finally, we recall that the Jstage_{gen} flag is based on a very heterogeneous

set of images in terms of wavelengths, depth, quality, and therefore results must be taken with caution.

4. Results II: Is the AGN Fraction among Ram-pressure-stripped Galaxies Higher than in Nonstripped Galaxies?

In the previous section we have quantified the incidence of AGNs in ram-pressure-stripped galaxies. We have seen that they represent 24% of the overall, both for GASP-RPS and LIT-RPS samples. In the following we will always exclude masses $< 10^9 M_\odot$, in all samples. Table 6 presents the AGN fractions in GASP-RPS and LIT-RPS separately for stellar masses $\geq 10^9 M_\odot$ and $\geq 10^{10} M_\odot$.²⁰ The fractions in the LIT-RPS sample are always higher than in GASP-RPS (0.29 versus 0.24 and 0.55 versus 0.46, respectively for the two mass bins), but are compatible within the binomial errors. Including also the four X-ray/radio AGNs in the literature, fractions are slightly higher. We note that also the stellar mass distributions of the two samples are similar (Figure 4), and indeed a Kolmogorov–Smirnov (KS) test cannot exclude that they are drawn from the same parent distribution.

¹⁹ The subsample of LIT-RPS galaxies with Jstage is too small to study trends with the length of the H α tails.

²⁰ From now on we exclude from this analysis ID345 at $z = 0.73$, considered a redshift outlier.

Table 4
Stellar Masses and AGN Classifications

Name	$\log(M_*/M_\odot)$	AGN	References
MIP001417–302303	9.6 Rawle et al. (2014)	0 Owers et al. (2012)	Owers et al. (2012); Rawle et al. (2014)
HLS001427–302344	10.9 Rawle et al. (2014)	1 Owers et al. (2012)	Owers et al. (2012); Rawle et al. (2014)
NGC 1566	10.8 Elagali et al. (2019)	1 Véron-Cetty & Véron (2006)	Elagali et al. (2019)
ID345	10.3 Boselli et al. (2019)	1 Boselli et al. (2019)	Boselli et al. (2019)
LEDA36382	9.5 Mendel et al. (2014)	0 SDSS (2004)	Gavazzi et al. (1995, 2001) Sivanandam et al. (2014); Boselli et al. (2018); Yagi et al. (2017)

Notes. Columns: (1) galaxy name; (2) logarithm of the stellar masses, adopting Chabrier (2003) IMF (references from which the values have been taken are reported below); (3) AGN classification (see Table 1) and related reference; (4) references which present a characterization of the galaxy as an RPS candidate. The four galaxies with classifications equal to 4 and 5 (e.g., where the AGN is spotted observing them in X and radio) resulted to be star-forming in the optics. In the text we analyze the consequence to change their AGN flag to 0. This table is published in its entirety in a machine-readable format. A portion is shown here for guidance regarding its form and content.

References. Abramson & Kenney (2014); Abramson et al. (2016); Best et al. (2012); Birchall et al. (2020); Boselli et al. (2005, 2006, 2015, 2016, 2018, 2019); Chemin et al. (2005); Chen et al. (2020); Chung et al. (2007, 2009); Chyży et al. (2007); Consolandi et al. (2017); Cortese et al. (2007); Cramer et al. (2020, 2019); Damas-Segovia et al. (2016); Davies et al. (2020); Decarli et al. (2007); Ebeling et al. (2019, 2014); Elagali et al. (2019); Fossati et al. (2012, 2016); Fruscione et al. (1990); Fumagalli et al. (2011, 2014); Gavazzi (1989); Gavazzi et al. (1984, 1995, 2001, 2017, 2018); Gu et al. (2013); Gullieuszik et al. (2020); Hester et al. (2010); Ho et al. (1997); Jáchym et al. (2014, 2017, 2019); Kalita et al. (2019); Kantharia et al. (2008); Kenney et al. (1995, 2004, 2008, 2014, 2015); Lee et al. (2017, 2018); Mahajan et al. (2010); McPartland et al. (2016); Mendel et al. (2014); Merluzzi et al. (2010, 2013, 2016); Minchin et al. (2019); Nucita et al. (2017); Oosterloo et al. (2005); Owen et al. (2006); Owers et al. (2012); Rahman et al. (2011); Rakshit et al. (2017); Rawle et al. (2014); Roberts et al. (2020); Ruszkowski et al. (2014); Salim et al. (2018, 2016); Scott et al. (2010); SDSS (2004); Sivanandam et al. (2010, 2014); Smith et al. (2010); Sobral et al. (2015); Stein et al. (2017); Stroe et al. (2020); Sun et al. (2005, 2006, 2007, 2010); Tschöke et al. (2001); Véron-Cetty & Véron (2003, 2006); Vollmer & Vollmer (2003); Vollmer et al. (2004, 2009); Wang et al. (2020); Weżgowiec et al. (2012); Yagi et al. (2010, 2013, 2017); Yoshida et al. (2002, 2004, 2012); Zhang et al. (2013).

(This table is available in its entirety in machine-readable form.)

Table 5
AGN Fractions for the LIT-RPS Sample

$N_{\text{AGN}}/N_{\text{TOT}}$	f_{AGN}	Jstage _{gen}	$\log(M_*/M_\odot)$
20/82 (24/82)	$0.24^{+0.05}_{-0.04}$ ($0.29^{+0.05}_{-0.05}$)	All	All
12/15 (12/15)	$0.80^{+0.08}_{-0.12}$ ($0.80^{+0.08}_{-0.12}$)	All	≥ 10.5
4/15 (5/15)	$0.27^{+0.13}_{-0.10}$ ($0.33^{+0.13}_{-0.11}$)	=0	All
2/10 (2/10)	$0.20^{+0.15}_{-0.10}$ ($0.20^{+0.15}_{-0.10}$)	=0.5	All
3/18 (4/18)	$0.17^{+0.11}_{-0.07}$ ($0.22^{+0.11}_{-0.08}$)	=1	All
8/30 (10/30)	$0.27^{+0.09}_{-0.07}$ ($0.33^{+0.09}_{-0.08}$)	=2	All

Note. Considering galaxies of different mass ranges and characterized by different Jstage_{gen}. Errors on fractions are binomial. Values outside/in brackets are the fractions computed ignoring/considering the four galaxies classified as AGNs based on radio and X data.

It is therefore appropriate to join the two RPS samples to obtain the largest possible statistics²¹ and derive the total AGN fractions: $0.27^{+0.04}_{-0.04}$ at masses $\geq 10^9 M_\odot$ and $0.51^{+0.07}_{-0.07}$ for masses $\geq 10^{10} M_\odot$. These fractions are high but less extreme than the fraction that would have been inferred from the P17b results, where 6/7 galaxies were AGNs with a corresponding fraction of $0.86^{+0.18}_{-0.09}$. This is due to the fact that the 2017 sample was composed of all massive Jstage = 2 galaxies, and as we have seen in the previous sections these are the most favorable conditions for AGN activity in ram-pressure-stripped galaxies.

We now aim at establishing whether the AGN frequency is connected to RPS and therefore we compare the measured fractions to those obtained exploiting the MaNGA-Ref sample, used as representative of non-ram-pressure-stripped field galaxies.

As for the other samples, also in MaNGA-Ref, AGNs are located preferentially among the most massive galaxies (right panel of Figure 2). The AGN fraction is $0.15^{+0.0122}_{-0.01}$ above $\log(M_*/M_\odot) \geq 9.0$ and $0.28^{+0.02}_{-0.02}$ for $\log(M_*/M_\odot) \geq 10.0$.

A KS test excludes that the MaNGA-Ref mass distribution is drawn from the same parent distribution of the GASP+LIT sample (Figure 4). Since the probability to find an AGN increases with galaxy mass, to properly compare the fractions obtained from MaNGA-Ref and ALL-RPS we need to control for the different mass distributions. We perform a bootstrap random extraction of the MaNGA sample to create 10,000 subsamples with the same mass distribution of the ALL-RPS sample matching the number of ALL-RPS galaxies in bins of 0.3 dex in stellar mass. For each of the extracted samples we compute the AGN fraction f_{AGN} . We repeat the random extraction considering separately two stellar mass ranges, $M_* \geq 10^9 M_\odot$ and $M_* \geq 10^{10} M_\odot$. Violin plots with the f_{AGN} distributions for the two mass ranges, their medians, and the 25th and 75th percentiles are shown in Figure 5. We find that the median f_{AGN} of the 10,000 realizations of mass-matched MaNGA galaxies are $f_{\text{AGN}} = 0.18$ for $M \geq 10^9 M_\odot$ and 0.35 for $M \geq 10^{10} M_\odot$. These values are lower than the corresponding values in the ALL-RPS sample, which are 0.27 and 0.51, respectively. In order to assess the significance of the difference between the RPS and non-RPS samples, we compute the pivotal confidence intervals of the bootstrap distribution and find that the mass-matched MaNGA fractions are lower than the ALL-RPS fractions at the 99.99% confidence level for galaxies with $M \geq 10^9 M_\odot$ (>99.99% if we include the four

²¹ Note that the galaxy JO147 appears in both samples, from now on we will just consider it once.

²² Previous MaNGA works (e.g., Sánchez et al. 2018) have found a significantly lower AGN incidence. However previous analysis has not applied any cut in sSFR as we do, and have adopted much more stringent definitions (emission line ratios above the Kewley demarcation lines considering all the BPT diagrams simultaneously and H α equivalent width $> 1.5 \text{ \AA}$ in the central regions) for AGNs, therefore results are not directly comparable.

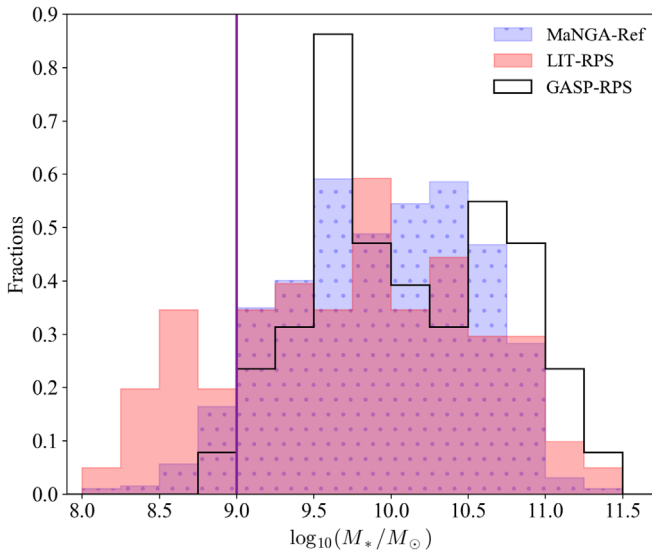


Figure 4. Normalized stellar mass distributions of the GASP (black histogram), MaNGA (purple-dotted histogram), and literature sample (light red histogram). For the Montecarlo, we have selected galaxies above the vertical-dotted line, i.e., with masses $\log(M_*/M_\odot) \geq 9$.

radio/X-ray AGNs), and at the 99.96% level for $M \geq 10^{10} M_\odot$ (>99.99% if the four radio/X-ray AGNs are included) (see Figure 5).

Since the three samples considered span slightly different redshift ranges, we performed the bootstrap random extractions also limiting all samples to $z \leq 0.075$ (the GASP redshift limit). Results remained unchanged as fractions are affected only at the 1% level at most. Finally, we also tried comparing mass-matched MaNGA samples separately with GASP-RPS and LIT-RPS. Though clearly the statistics decrease, we still find high probabilities that the mass-matched MaNGA sample has lower AGN fractions than the RPS samples (81.4% and 95.4% for GASP-RPS in the two mass ranges, and >99.99% for both LIT-RPS samples).

From our analysis the incidence of AGN activity among ram-pressure-stripped galaxies is significantly higher than that in the MaNGA field control sample. A ram-pressure-stripped galaxy has a 1.5 times higher probability to host an AGN than a similar non-ram-pressure-stripped galaxy. This effect is not driven by different stellar mass distributions and points to a connection between RPS and AGN activity.

A larger (of the order of hundreds), homogeneous sample of ram-pressure-stripped galaxies with integral-field spectroscopy would be needed to place these results on more solid ground. Since this is currently unavailable, the analysis presented here collects the best available data sets for addressing the question of the AGN–RPS connection. There are however several caveats worth stressing.

First of all, the AGN fraction depends strongly on the criteria adopted when using the BPT diagram. In this paper, we are including both LINER-like and Seyfert AGN, in order to capture also low luminosity AGN. This is done in all samples considered in a similar manner, so it should not affect the relative incidence and the main conclusions of this work, but the pure AGN fractions will strongly depend on the initial choice.

Second, although great care has been taken to ensure the most homogeneous analysis possible, the data sets are clearly nonhomogeneous. Even GASP and MaNGA, which are both

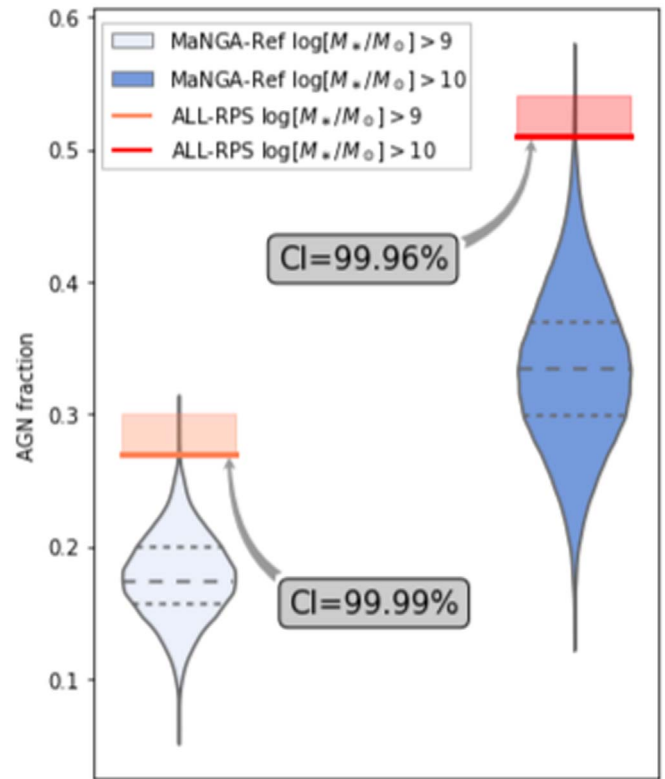


Figure 5. Comparison of the AGN fraction in the different samples. Red and orange lines refer to the ALL-RPS sample: the AGN fraction for galaxies with $M_* \geq 10^9 M_\odot$ is shown by the thick orange line, that for galaxies with $M_* \geq 10^{10} M_\odot$ by the thick red line. The matched shaded areas indicate by how much fractions change if we consider also the AGN classified on the basis of X-ray or radio data (see text for details). Blue and light blue violin plots refer to the MaNGA-Ref sample, for the two mass bins as indicated in the labels. They show the probability density of the bootstrap random extractions mass-matched to the ALL-RPS sample, at different AGN fraction values, smoothed by a kernel density estimator. Gray horizontal dashed and dotted lines represent median values and 25% and 75% percentiles of the AGN fraction, respectively. Values of the pivotal confidence intervals of the bootstrap distribution are also reported: the mass-matched MaNGA fractions are lower than the ALL-RPS fractions at the 99.99% confidence level for galaxies with $M \geq 10^9 M_\odot$ and at the 99.96% level for $M \geq 10^{10} M_\odot$.

based on integral-field data for every galaxy, have been observed with different instruments, thus have different resolutions, spaxel size, etc., and span a slightly different redshift range (see above for invariance of AGN fractions with the redshift interval adopted). The literature sample, obviously, is in itself very heterogeneous, with the spectroscopic information coming from many different sources. The results shown in this paper should therefore be taken with caution and revisited once large homogeneous samples will become available.

Third, in principle, it is possible that the high AGN fraction we observe in ram-pressure-stripped galaxies is not a consequence of RPS itself. If the AGN incidence in cluster star-forming galaxies was higher in general than in similar galaxies in the field, the differences with respect to MaNGA would go in the same direction as what we observe. However, as mentioned also above, the AGN fraction in the GASP non-RPS sample is small (2/49) (Vulcani et al. 2021). This sample is composed both of cluster and field undisturbed galaxies. If we consider only the GASP cluster control sample (star-forming and late-types), there is no AGN (B. Poggianti et al.

Table 6
AGN Fractions and Binomial Errorbars for the GASP-RPS, LIT-RPS, and ALL-RPS Samples in Two Different Mass Bins

$\log(M_*/M_\odot)$	GASP-RPS		LIT-RPS		ALL-RPS	
	$N_{\text{AGN}}/N_{\text{TOT}}$	f_{AGN}	$N_{\text{AGN}}/N_{\text{TOT}}$	f_{AGN}	$N_{\text{AGN}}/N_{\text{TOT}}$	f_{AGN}
≥ 9.0	12/50	$0.24^{+0.07}_{-0.06}$	19/65(23/65)	$0.29^{+0.06}_{-0.05}$ ($0.35^{+0.06}_{-0.06}$)	31/115(35/115)	$0.27^{+0.04}_{-0.04}$ ($0.30^{+0.04}_{-0.04}$)
≥ 10.0	12/25	$0.46^{+0.10}_{-0.09}$	17/31(19/31)	$0.55^{+0.09}_{-0.09}$ ($0.61^{+0.08}_{-0.09}$)	29/57(31/57)	$0.51^{+0.07}_{-0.07}$ ($0.54^{+0.07}_{-0.07}$)

Note. For the LIT-RPS and ALL-RPS samples, values in parentheses are obtained considering also galaxies identified as AGNs on the basis of X-ray or radio data.

2021, in preparation). So, this caveat is unlikely to be responsible for our results.

Finally, we note that we are not studying the global AGN fraction in clusters, but the occurrence of AGN activity in a very specific class of cluster galaxies: those with clear signs of RPS, which are all star-forming and late-type galaxies and thus represent a small fraction of the total cluster galaxy population that is dominated by early-type galaxies. Therefore, our results cannot be used to infer the total AGN fraction in clusters and not necessarily show similar trends.

5. Summary

In this paper we have investigated the occurrence of AGN activity in ram-pressure-stripped galaxies in local clusters, comparing it with the AGN frequency in a control sample of field galaxies. In all cases, we rely on BPT diagnostic diagrams based on the [N II] line. All the galaxies analyzed in this paper are star-forming and morphologically late-type galaxies.

First, we assembled two samples of ram-pressure-stripped galaxies. We have used the MUSE data of 51 galaxies observed in the context of the GASP survey (GASP-RPS) finding a Seyfert 2 and 4 LINER-like AGN hosts previously unknown, in addition to the seven galaxies already discussed in P17b and Fritz et al. (2017). We have then conducted a search in the literature assembling a sample of 82 ram-pressure-stripped galaxies for which it was possible to retrieve information on their nuclear activity (either from IFU or slit/fiber) (LIT-RPS).

We find similar fractions of AGNs in GASP and in literature ram-pressure-stripped galaxies, with the AGN incidence being slightly higher in the literature than in GASP, but consistent within the uncertainties. Overall, the AGN fraction in the total GASP-RPS+LIT-RPS sample is $0.27^{+0.04}_{-0.04}$ at masses $M_* \geq 10^9 M_\odot$ and $0.51^{+0.07}_{-0.07}$ at $M_* \geq 10^{10} M_\odot$. Thus, more than half of the $\geq 10^{10} M_\odot$ ram-pressure-stripped galaxies show AGN activity.

We then compare these findings with those for a sample of galaxies drawn from the MaNGA survey and inhabiting dark matter haloes with masses $\leq 10^{13} M_\odot$. With this halo mass cut we ensure that rich groups and clusters are excluded, hence these galaxies are not undergoing significant RPS and this can serve as a control field sample. We perform a bootstrap random extraction from the MaNGA sample to create 10,000 realizations with the same stellar mass distribution of the RPS sample.

Our two main results can be summarized as follows:

1. The great majority of galaxies hosting an AGN, in all three samples considered, are high-mass galaxies. There are just very few galaxies with an AGN at a mass below $10^{10} M_\odot$ (none below $10^{10.5} M_\odot$ in GASP). As a consequence, the AGN fractions are higher above these limits, and very low below. Another factor that could be playing a role is the ram-pressure strength or phase

(Jstage): the highest AGN fractions are observed among the most strongly ram-pressure-stripped galaxies with the longest tails. However, with the current samples it is hard to disentangle between mass and Jstage effects.

2. Even after matching the galaxy mass distributions, the AGN incidence in the field MaNGA sample is lower than in the RPS sample at the $\geq 99.96\%$ confidence level. Overall, a ram-pressure-stripped galaxy has a 1.5 times higher probability to host an AGN than a similar non-ram-pressure-stripped galaxy. This supports the hypothesis that ram pressure can trigger the AGN activity.

We thank the Referee for the useful suggestions that improved the presentation of the work. We warmly thank Jong-Ho Shinn from the Korea Astronomy and Space Science Institute for useful discussion regarding the statistical analysis. G.P. thanks A. Werle for the helpful discussion. Based on observations collected at the European Organization for Astronomical Research in the Southern Hemisphere under ESO program 196.B-0578. This project has received funding from the European Research Council (ERC) under the European Union's Horizon 2020 research and innovation program (grant agreement No. 833824). We acknowledge the financial contribution from the grant PRIN MIUR 2017 n.20173ML3WW_001 (PI: Cimatti), from the INAF mainstream funding program (PI: Vulcani), and from the agreement ASI-INAF n.2017-14- H.0 (PI: A. Moretti). Y.J. acknowledges financial support from CONICYT PAI (Concurso Nacional de Inserción en la Academia 2017) grant No. 79170132 and FONDECYT Iniciación 2018 grant No. 11180558. J.F. acknowledges financial support from the UNAM- DGAPA-PAPIIT IN111620 grant, México.

Appendix Mass Estimates











To compute stellar masses for those galaxies for which they are missing in the literature, we use the Bell et al. (2001) relation between the mass-to-light ratio of a galaxy and its color:

$$\log\left(\frac{M}{L_\lambda}\right) = a_\lambda + b_\lambda \cdot \text{COL}, \quad (\text{A1})$$

where L_λ is the luminosity in a band, indicated with λ , COL is a photometric color and a_λ and b_λ are coefficients depending on both λ and COL. For our calculations, we used the Bell et al. (2001) tables for a solar metallicity $Z=0.02$ and a Bruzual & Charlot (2003) SSP model, converting from a Salpeter (1955) to a Chabrier (2003) IMF subtracting a factor -0.24 . For one galaxy, 235144-260358 (Cortese et al. 2007), in order to use the formula (A1) we first converted HST magnitudes to a UVB photometric system with the use of

calibration equations for the Advanced Camera for Surveys (ACS) presented in Sirianni et al. (2005). We assume a typical 0.3 dex uncertainty on the computed stellar masses, which we take as bin size of the stellar mass distribution.

ORCID iDs

Giorgia Peluso  <https://orcid.org/0000-0001-5766-7154>
 Benedetta Vulcani  <https://orcid.org/0000-0003-0980-1499>
 Bianca M. Poggianti  <https://orcid.org/0000-0001-8751-8360>
 Alessia Moretti  <https://orcid.org/0000-0002-1688-482X>
 Mario Radovich  <https://orcid.org/0000-0002-3585-866X>
 Rory Smith  <https://orcid.org/0000-0001-5303-6830>
 Yara L. Jaffé  <https://orcid.org/0000-0003-2150-1130>
 Marco Gullieuszik  <https://orcid.org/0000-0002-7296-9780>
 Jacopo Fritz  <https://orcid.org/0000-0002-7042-1965>
 Alessandro Ignesti  <https://orcid.org/0000-0003-1581-0092>

References

- Abazajian, K. N., Adelman-McCarthy, J. K., Agüeros, M. A., et al. 2009, *ApJS*, **182**, 543
- Abramson, A., Kenney, J., Crowl, H., & Tal, T. 2016, *AJ*, **152**, 32
- Abramson, A., & Kenney, J. D. P. 2014, *AJ*, **147**, 63
- Aguado, D. S., Ahumada, R., Almeida, A., et al. 2019, *ApJS*, **240**, 23
- Aihara, H., Prieto, C. A., An, D., et al. 2011, *ApJS*, **193**, 29
- Amiri, A., Tavasoli, S., & Zotti, G. D. 2019, *ApJ*, **874**, 140
- Argudo-Fernández, M., Lacerna, I., Puertas, S. D., et al. 2018, *A&A*, **620**, A113
- Arnold, T. J., Martini, P., Mulchaey, J. S., Berti, A., & Jeltema, T. E. 2009, *ApJ*, **707**, 1691
- Bahcall, J. N., Kirhakos, S., Saxe, D. H., & Schneider, D. P. 1997, *ApJ*, **479**, 642
- Baldwin, J. A., Phillips, M. M., Terlevich, R., et al. 1981, *PASP*, **93**, 5
- Bekki, K. 2014, *MNRAS*, **438**, 444
- Bell, E. F., de Jong, R. S., Bell, E. F., & de Jong, R. S. 2001, *ApJ*, **550**, 212
- Bellhouse, C., McGee, S. L., Smith, R., et al. 2021, *MNRAS*, **500**, 1285
- Best, P. N., Heckman, T. M., Best, P. N., & Heckman, T. M. 2012, *MNRAS*, **421**, 1569
- Best, P. N., von der Linden, A., Kauffmann, G., et al. 2007, *MNRAS*, **379**, 894
- Birchall, K. L., Watson, M. G., Aird, J., et al. 2020, *MNRAS*, **492**, 2268
- Boselli, A., Boissier, S., Cortese, L., et al. 2005, *ApJL*, **623**, L13
- Boselli, A., Boissier, S., Cortese, L., et al. 2006, *ApJ*, **651**, 811
- Boselli, A., Cuillandre, J. C., Fossati, M., et al. 2016, *A&A*, **587**, A68
- Boselli, A., Epinat, B., Contini, T., et al. 2019, *A&A*, **631**, A114
- Boselli, A., Fossati, M., Cuillandre, J. C., et al. 2018, *A&A*, **615**, A114
- Boselli, A., Fossati, M., Gavazzi, G., et al. 2015, *A&A*, **579**, A102
- Boselli, A., Fossati, M., & Sun, M. 2021, arXiv:2109.13614
- Brinchmann, J., Charlot, S., Heckman, T. M., et al. 2004, arXiv:abs/astro-ph/0406220
- Bruzual, G., & Charlot, S. 2003, *MNRAS*, **344**, 1000
- Bundy, K. 2015, *IAUS*, **311**, 100
- Caglar, T., Burtscher, L., Brandl, B., et al. 2020, *A&A*, **634**, A114
- Calvi, R., Poggianti, B. M., Vulcani, B., et al. 2011, *MNRAS*, **416**, 727
- Canalizo, G., & Stockton, A. 2001, *ApJ*, **555**, 719
- Chabrier, G. 2003, *PASP*, **115**, 763
- Chemin, L., Cayatte, V., Balkowski, C., et al. 2005, *A&A*, **436**, 469
- Chen, H., Sun, M., Yagi, M., et al. 2020, *MNRAS*, **496**, 4654
- Chung, A., van Gorkom, J. H., Kenney, J. D. P., et al. 2009, *AJ*, **138**, 1741
- Chung, A., van Gorkom, J. H., Kenney, J. D. P., & Vollmer, B. 2007, *ApJL*, **659**, L115
- Chyży, K. T., Ehle, M., Beck, R., et al. 2007, *A&A*, **474**, 415
- Coldwell, G. V., Pereyra, L., Alonso, S., et al. 2017, *MNRAS*, **467**, 3338
- Consolandi, G., Gavazzi, G., Fossati, M., et al. 2017, *A&A*, **606**, A83
- Cortese, L., Marcellac, D., Richard, J., et al. 2007, *MNRAS*, **376**, 157
- Cramer, W. J., Kenney, J. D. P., Cortes, J. R., et al. 2020, *ApJ*, **901**, 95
- Cramer, W. J., Kenney, J. D. P., Sun, M., et al. 2019, *ApJ*, **870**, 63
- Crowl, H. H., & Kenney, J. D. P. 2006, *ApJ*, **649**, L75
- Damas-Segovia, A., Beck, R., Vollmer, B., et al. 2016, *ApJ*, **824**, 30
- Davies, R., Baron, D., Shimizu, T., et al. 2020, *MNRAS*, **498**, 4150
- Decarli, R., Gavazzi, G., Arosio, I., et al. 2007, *MNRAS*, **381**, 136
- Dressler, A., Thompson, I. B., & Shectman, S. A. 1985, *ApJ*, **288**, 481
- Ebeling, H., Kalita, B. S., Ebeling, H., & Kalita, B. S. 2019, *ApJ*, **882**, 127
- Ebeling, H., Stephenson, L. N., Edge, A. C., et al. 2014, *ApJL*, **781**, L40
- Ehlert, S., von der Linden, A., Allen, S. W., et al. 2014, *MNRAS*, **437**, 1942
- Elagali, A., Staveley-Smith, L., Rhee, J., et al. 2019, *MNRAS*, **487**, 2797
- Evans, I. N., Primini, F. A., Miller, J. B., et al. 2020, AAS Meeting, **235**, 154.05
- Fasano, G., Marmo, C., Varela, J., et al. 2006, *A&A*, **445**, 805
- Fossati, M., Fumagalli, M., Boselli, A., et al. 2016, *MNRAS*, **455**, 2028
- Fossati, M., Gavazzi, G., Boselli, A., et al. 2012, *A&A*, **544**, A128
- Fritz, J., Moretti, A., Gullieuszik, M., et al. 2017, *ApJ*, **848**, 132
- Fruscione, A., Gavazzi, G., Fruscione, A., & Gavazzi, G. 1990, *A&A*, **230**, 293
- Fumagalli, M., Fossati, M., Hau, G. K. T., et al. 2014, *MNRAS*, **445**, 4335
- Fumagalli, M., Gavazzi, G., Scaramella, R., et al. 2011, *A&A*, **528**, A46
- Gavazzi, G. 1989, *ApJ*, **346**, 59
- Gavazzi, G., Boselli, A., Mayer, L., et al. 2001, *ApJL*, **563**, L23
- Gavazzi, G., Consolandi, G., Gutierrez, M. L., et al. 2018, *A&A*, **618**, A130
- Gavazzi, G., Consolandi, G., Yagi, M., et al. 2017, *A&A*, **606**, A131
- Gavazzi, G., Contursi, A., Carrasco, L., et al. 1995, *A&A*, **304**, 325
- Gavazzi, G., Tarengi, M., Jaffe, W., et al. 1984, *A&A*, **137**, 235
- George, K., Poggianti, B. M., Bellhouse, C., et al. 2019, *MNRAS*, **487**, 3102
- Gilmour, R., Gray, M. E., Almaini, O., et al. 2007, *MNRAS*, **380**, 1467
- Gordon, Y. A., Pimbblet, K. A., Owers, M. S., et al. 2018, *MNRAS*, **475**, 4223
- Gu, L., Yagi, M., Nakazawa, K., et al. 2013, *ApJL*, **777**, L36
- Gullieuszik, M., Poggianti, B., Fasano, G., et al. 2015, *A&A*, **581**, A41
- Gullieuszik, M., Poggianti, B. M., McGee, S. L., et al. 2020, *ApJ*, **899**, 13
- Gunn, J. E., Gott, J., & Richard, I. 1972, *ApJ*, **176**, 1
- Gunn, J. E., Siegmund, W. A., Mannery, E. J., et al. 2006, *AJ*, **131**, 2332
- Hernández-Toledo, H. M., Vázquez-Mata, J. A., Martínez-Vázquez, L. A., et al. 2010, *AJ*, **139**, 2525
- Hester, J. A. 2006, *ApJ*, **647**, 910
- Hester, J. A., Seibert, M., Neill, J. D., et al. 2010, *ApJL*, **716**, L14
- Ho, L. C., Filippenko, A. V., & Sargent, W. L. W. 1997, *ApJS*, **112**, 315
- Hwang, H. S., Park, C., Elbaz, D., & Choi, Y.-Y. 2012, *A&A*, **538**, A15
- Jáchym, P., Combes, F., Cortese, L., et al. 2014, *ApJ*, **792**, 11
- Jáchym, P., Kenney, J. D. P., Sun, M., et al. 2019, *ApJ*, **883**, 145
- Jáchym, P., Sun, M., Kenney, J. D. P., et al. 2017, *ApJ*, **839**, 114
- Jaffé, Y. L., Poggianti, B. M., Moretti, A., et al. 2018, *MNRAS*, **476**, 4753
- Juneau, S., Dickinson, M., Alexander, D. M., et al. 2011, *ApJ*, **736**, 104
- Kalita, B. S., Ebeling, H., Kalita, B. S., & Ebeling, H. 2019, *ApJ*, **887**, 158
- Kantharia, N. G., Rao, A. P., Sirothia, S. K., et al. 2008, *MNRAS*, **383**, 173
- Kapferer, W., Sluka, C., Schindler, S., Ferrari, C., & Ziegler, B. 2009, *A&A*, **499**, 87
- Kauffmann, G., Heckman, T. M., Tremonti, C., et al. 2003, *MNRAS*, **346**, 1055
- Kauffmann, G., White, S. D. M., Heckman, T. M., et al. 2004, *MNRAS*, **353**, 713
- Kenney, J. D., Abramson, A., & Bravo-Alfaro, H. 2015, *AJ*, **150**, 59
- Kenney, J. D. P., Geha, M., Jáchym, P., et al. 2014, *ApJ*, **780**, 119
- Kenney, J. D. P., Rubin, V. C., Planesas, P., & Young, J. S. 1995, *ApJ*, **438**, 135
- Kenney, J. D. P., Tal, T., Crowl, H. H., et al. 2008, *ApJL*, **687**, L69
- Kenney, J. D. P., van Gorkom, J. H., Vollmer, B., et al. 2004, *AJ*, **127**, 3361
- Kewley, L. J., Dopita, M. A., Sutherland, R. S., et al. 2001, *ApJ*, **556**, 121
- Kormendy, J., Ho, L. C., Kormendy, J., & Ho, L. C. 2013, *ARA&A*, **51**, 511
- Koulouridis, E., Ricci, M., Giles, P., et al. 2018, *A&A*, **620**, A20
- Kronberger, T., Kapferer, W., Ferrari, C., Unterguggenberger, S., & Schindler, S. 2008, *A&A*, **481**, 337
- Law, D. R., Ji, X., Belfiore, F., et al. 2021, *ApJ*, **915**, 35
- Lee, B., Chung, A., Lee, B., & Chung, A. 2018, *ApJL*, **866**, L10
- Lee, B., Chung, A., Tonnesen, S., et al. 2017, *MNRAS*, **466**, 1382
- Lehmer, B. D., Brandt, W. N., Alexander, D. M., et al. 2007, *ApJ*, **657**, 681
- Letawe, Y., Letawe, G., & Magain, P. 2010, *MNRAS*, **403**, 2088
- Lopes, P. A. A., Ribeiro, A. L. B., Rembold, S. B., et al. 2017, *MNRAS*, **472**, 409
- Magliocchetti, M., Pentericci, L., Cirasuolo, M., et al. 2020, *MNRAS*, **493**, 3838
- Magliocchetti, M., Popesso, P., Brusa, M., & Salvato, M. 2018, in The 13th Italian Meeting on Active Galactic Nuclei, Beauty and the Beast, ed. G. Ghisellini et al. (Rome: INAF), 26
- Mahajan, S., Haines, C. P., Raychaudhury, S., et al. 2010, *MNRAS*, **404**, 1745
- Maier, C., Haines, C. P., & Ziegler, B. L. 2022, *A&A*, **658**, A190
- Man, Z.-y., Peng, Y.-j., Kong, X., et al. 2019, *MNRAS*, **488**, 89
- Martini, P., Miller, E. D., Brodwin, M., et al. 2013, *ApJ*, **768**, 1
- Martini, P., Mulchaey, J. S., Kelson, D. D., et al. 2007, *ApJ*, **664**, 761

- Marziani, P., D’Onofrio, M., Bettoni, D., et al. 2017, *A&A*, **599**, A83
- McPartland, C., Ebeling, H., Roediger, E., et al. 2016, *MNRAS*, **455**, 2994
- Mendel, J. T., Simard, L., Palmer, M., et al. 2014, *ApJS*, **210**, 3
- Merluzzi, P., Busarello, G., Dopita, M. A., et al. 2013, *MNRAS*, **429**, 1747
- Merluzzi, P., Busarello, G., Dopita, M. A., et al. 2016, *MNRAS*, **460**, 3345
- Merluzzi, P., Mercurio, A., Haines, C. P., et al. 2010, *MNRAS*, **402**, 753
- Miller, C. J., Nichol, R. C., Gomez, P., Hopkins, A., & Bernardi, M. 2003, *ApJ*, **597**, 142
- Minchin, R. F., Taylor, R., Köppen, J., et al. 2019, *AJ*, **158**, 121
- Montero-Dorta, A. D., Croton, D. J., Yan, R., et al. 2009, *MNRAS*, **392**, 125
- Moretti, A., Poggianti, B. M., Gullieuszik, M., et al. 2018, *MNRAS*, **475**, 4055
- Navarro, J. F., Frenk, C. S., White, S. D. M., et al. 1997, *ApJ*, **490**, 493
- Nucita, A. A., Manni, L., Paolis, F. D., et al. 2017, *ApJ*, **837**, 66
- Oosterloo, T., van Gorkom, J., Oosterloo, T., & van Gorkom, J. 2005, *A&A*, **437**, L19
- Owen, F. N., Keel, W. C., Wang, Q. D., et al. 2006, *AJ*, **131**, 1974
- Owers, M. S., Couch, W. J., Nulsen, P. E. J., et al. 2012, *ApJL*, **750**, L23
- Pappalardo, C., Bianchi, S., Corbelli, E., et al. 2012, *A&A*, **545**, A75
- Pimblett, K. A., Shabala, S. S., Haines, C. P., Fraser-McKelvie, A., & Floyd, D. J. 2013, *MNRAS*, **429**, 1827
- Poggianti, B. M., Gullieuszik, M., Tonnesen, S., et al. 2019, *MNRAS*, **482**, 4466
- Poggianti, B. M., Jaffé, Y. L., Moretti, A., et al. 2017b, *Natur*, **548**, 304
- Poggianti, B. M., Moretti, A., Gullieuszik, M., et al. 2017a, *ApJ*, **844**, 48
- Radovich, M., Poggianti, B., Jaffé, Y. L., et al. 2019, *MNRAS*, **486**, 486
- Rahman, N., Bolatto, A. D., Wong, T., et al. 2011, *ApJ*, **730**, 72
- Rakshit, S., Stalin, C. S., Chand, H., et al. 2017, *ApJS*, **229**, 39
- Ramos-Martínez, M., Gómez, G. C., Ángeles, P.-V., et al. 2018, *MNRAS*, **476**, 3781
- Rawle, T. D., Altieri, B., Egami, E., et al. 2014, *MNRAS*, **442**, 196
- Ricarte, A., Tremmel, M., Natarajan, P., et al. 2020, *ApJL*, **895**, L8
- Roberts, I. D., Parker, L. C., Roberts, I. D., & Parker, L. C. 2020, *MNRAS*, **495**, 554
- Rodríguez del Pino, B., Aragón-Salamanca, A., Chies-Santos, A. L., et al. 2017, *MNRAS*, **467**, 4200
- Roman-Oliveira, F. V., Chies-Santos, A. L., del Pino, B. R., et al. 2018, *MNRAS*, **484**, 892
- Ruszkowski, M., Brüggén, M., Lee, D., & Shin, M. S. 2014, *ApJ*, **784**, 75
- Sabater, J., Best, P. N., & Argudo-Fernández, M. 2013, *MNRAS*, **430**, 638
- Salim, S., Boquien, M., Lee, J. C., et al. 2018, *ApJ*, **859**, 11
- Salim, S., Lee, J. C., Janowiecki, S., et al. 2016, *ApJS*, **227**, 2
- Salpeter, E. E. 1955, *ApJ*, **121**, 161
- Sánchez, S. F., Avila-Reese, V., Hernandez-Toledo, H., et al. 2018, *RMxAA*, **54**, 217
- Sánchez, S. F., Perez, E., Sánchez-Blázquez, P., et al. 2016a, *RMxAA*, **52**, 21
- Sánchez, S. F., Pérez, E., Sánchez-Blázquez, P., et al. 2016b, *RMxAA*, **52**, 171
- Sanders, D. B., Soifer, B. T., Elias, J. H., et al. 1988, *ApJ*, **325**, 74
- Schulz, S., & Struck, C. 2001, *MNRAS*, **328**, 185
- Scott, T. C., Bravo-Alfaro, H., Brinks, E., et al. 2010, *MNRAS*, **403**, 1175
- Scott, T. C., Usero, A., Brinks, E., et al. 2013, *MNRAS*, **429**, 221
- SDSS. 2004, Galaxy Properties for DR8 spectra from MPA-JHU|SDSS, https://www.sdss.org/dr12/spectro/galaxy_mpajhu/
- Sharp, R. G., Bland-Hawthorn, J., Sharp, R. G., & Bland-Hawthorn, J. 2010, *ApJ*, **711**, 818
- Silverman, J. D., & David, J. 2015, *IAUGA Meeting*, **29**, 2246407
- Silverman, J. D., Kovač, K., Knobel, C., et al. 2009, *ApJ*, **695**, 171
- Sirianni, M., Jee, M. J., Benítez, N., et al. 2005, *PASP*, **117**, 1049
- Sivakoff, G. R., Martini, P., Zabludoff, A. I., et al. 2008, *ApJ*, **682**, 803
- Sivanandam, S., Rieke, M. J., & Rieke, G. H. 2010, *ApJ*, **717**, 147
- Sivanandam, S., Rieke, M. J., Rieke, G. H., et al. 2014, *ApJ*, **796**, 89
- Smee, S. A., Gunn, J. E., Uomoto, A., et al. 2013, *AJ*, **146**, 32
- Smirnova, A. A., Moiseev, A. V., & Afanasiev, V. L. 2010, *MNRAS*, **408**, 400
- Smith, R. J., Lucey, J. R., Hammer, D., et al. 2010, *MNRAS*, **408**, 1417
- Sobral, D., Stroe, A., Dawson, W. A., et al. 2015, *MNRAS*, **450**, 630
- Stein, Y., Bomans, D. J., Ferguson, A. M. N., et al. 2017, *A&A*, **605**, A5
- Stroe, A., Hussaini, M., Husemann, B., et al. 2020, *ApJL*, **905**, L22
- Sun, M., Donahue, M., Roediger, E., et al. 2010, *ApJ*, **708**, 946
- Sun, M., Donahue, M., & Voit, G. M. 2007, *ApJ*, **671**, 190
- Sun, M., Jones, C., Forman, W., et al. 2006, *ApJL*, **637**, L81
- Sun, M., Vikhlinin, A., Sun, M., & Vikhlinin, A. 2005, *ApJ*, **621**, 718
- Tempel, E., Tamm, A., Gramann, M., et al. 2014, *A&A*, **566**, A1
- Tonnesen, S., Bryan, G. L., Tonnesen, S., & Bryan, G. L. 2009, *ApJ*, **694**, 789
- Tonnesen, S., Bryan, G. L., & van Gorkom, J. H. 2007, *ApJ*, **671**, 1434
- Tremonti, C. A., Heckman, T. M., Kauffmann, G., et al. 2004, *ApJ*, **613**, 898
- Tschöke, D., Bomans, D. J., Hensler, G., et al. 2001, *A&A*, **380**, 40
- Urrutia, T., Lacy, M., & Becker, R. H. 2008, *ApJ*, **674**, 80
- van Gorkom, J. H. 2004, Clusters of Galaxies: Probes of Cosmological Structure and Galaxy Evolution ed. J. S. Mulchaey, A. Dressler, & A. Oemler., 305, arXiv:astro-ph/0308209
- Véron-Cetty, M. P., & Véron, P. 2003, *A&A*, **412**, 399
- Véron-Cetty, M. P., & Véron, P. 2006, *A&A*, **455**, 773
- Vollmer, B., Beck, R., Kenney, J. D. P., et al. 2004, *AJ*, **127**, 3375
- Vollmer, B., Cayatte, V., Balkowski, C., & Duschl, W. J. 2001, *ApJ*, **561**, 708
- Vollmer, B., Soida, M., Beck, R., et al. 2013, *A&A*, **553**, A116
- Vollmer, B., Soida, M., Chung, A., et al. 2009, *A&A*, **496**, 669
- Vollmer, B., & Vollmer, B. 2003, *A&A*, **398**, 525
- von der Linden, A., Wild, V., Kauffmann, G., White, S. D. M., & Weinmann, S. 2010, *MNRAS*, **404**, 1231
- Vulcani, B., Fritz, J., Poggianti, B. M., et al. 2020, *ApJ*, **892**, 146
- Vulcani, B., Poggianti, B. M., Gullieuszik, M., et al. 2018, *ApJ*, **866**, L25
- Vulcani, B., Poggianti, B. M., Moretti, A., et al. 2021, *ApJ*, **914**, 27
- Wang, J., Xu, W., Lee, B., et al. 2020, *ApJ*, **903**, 103
- Weżgowiec, M., Bomans, D. J., Ehle, M., et al. 2012, *A&A*, **544**, A99
- Webb, N. A., Coriat, M., Traulsen, I., et al. 2020, *A&A*, **641**, A136
- Winkler, H., & Winkler, H. 1992, *MNRAS*, **257**, 677
- Yagi, M., Gu, L., Fujita, Y., et al. 2013, *ApJ*, **778**, 91
- Yagi, M., Yoshida, M., Gavazzi, G., et al. 2017, *ApJ*, **839**, 65
- Yagi, M., Yoshida, M., Komiyama, Y., et al. 2010, *AJ*, **140**, 1814
- Yang, X., Mo, H. J., van den Bosch, F. C., et al. 2007, *ApJ*, **671**, 153
- Yoshida, M., Yagi, M., Komiyama, Y., et al. 2012, *ApJ*, **749**, 43
- Yoshida, M., Yagi, M., Okamura, S., et al. 2002, *ApJ*, **567**, 118
- Yoshida, M., Yagi, M., Okamura, S., et al. 2004, *IAUS*, **217**, 386
- Zhang, B., Sun, M., Ji, L., et al. 2013, *ApJ*, **777**, 122